Eur. Phys. J. A **9**, 397–410 (2000)

THE EUROPEAN PHYSICAL JOURNAL A

Production of charged pions, kaons and antikaons in relativistic C + C and C + Au collisions

F. Laue[1], I. Böttcher[3], M. Dębowski[5], A. Förster[2], E. Grosse[6,7], P. Koczoń[1], B. Kohlmeyer[3], M. Mang[1], M. Menzel[3], L. Naumann[6], H. Oeschler[2], F. Pühlhofer[3], E. Schwab[1], P. Senger[1,a], Y. Shin[4], J. Speer[3], H. Ströbele[4], C. Sturm[2], G. Surówka[1,5], F. Uhlig[2], A. Wagner[6], and W. Waluś[5]
(KaoS Collaboration)

[1] Gesellschaft für Schwerionenforschung, D-64220 Darmstadt, Germany
[2] Technische Universität Darmstadt, D-64289 Darmstadt, Germany
[3] Phillips Universität, D-35037 Marburg, Germany
[4] Johann Wolfgang Goethe Universität, D-60325 Frankfurt am Main, Germany
[5] Jagiellonian University, PL-30059 Kraków, Poland
[6] Forschungszentrum Rossendorf, D-01314 Dresden, Germany
[7] Technische Universität Dresden, D-01314 Dresden, Germany

Received: 10 December 1999
Communicated by D. Guerreau

Abstract. Production cross-sections of charged pions, kaons and antikaons have been measured in C+C and C+Au collisions at beam energies of 1.0 and 1.8 AGeV for different polar emission angles. The kaon and antikaon energy spectra can be described by Boltzmann distributions whereas the pion spectra exhibit an additional enhancement at low energies. The pion multiplicity per participating nucleon $M(\pi^+)/\langle A_{\rm part}\rangle$ is a factor of about 3 smaller in C+Au than in C+C collisions at 1.0 AGeV whereas it differs only little for the C and the Au target at a beam energy of 1.8 AGeV. The K^+ multiplicities per participating nucleon $M(K^+)/\langle A_{\rm part}\rangle$ are independent of the target size at 1 AGeV and at 1.8 AGeV. The K^- multiplicity per participating nucleon $M(K^-)/\langle A_{\rm part}\rangle$ is reduced by a factor of about 2 in C+Au as compared to C+C collisions at 1.8 AGeV. This effect might be caused by the absorption of antikaons in the heavy target nucleus. Transport model calculations underestimate the K^-/K^+ ratio for C+C collisions at 1.8 AGeV by a factor of about 4 if in-medium modifications of K-mesons are neglected.

PACS. 25.75.Dw Particle and resonance production

1 Introduction

The study of meson production and propagation in relativistic nucleus-nucleus collisions has become an important experimental tool for the investigation of the properties of nuclear matter at high densities and of the hadron self-energy in a dense nuclear medium [1–3]. The pion multiplicity measured in heavy-ion experiments at the BEVALAC has been correlated with the thermal energy of the fireball in order to extract information on the nuclear matter equation of state [4]. In a more advanced approach, the production of kaons in nucleus-nucleus collisions at beam energies below the threshold for free NN collisions ($E_{\rm beam} = 1.58$ GeV for NN→$K^+\Lambda$N) is used to probe the compressibility of nuclear matter [5,6].

The properties of strange mesons in a medium of finite baryon density are essential for our understanding of strong interactions. According to various theoretical approaches, antikaons feel strong attractive forces in the nuclear medium whereas the in-medium kaon-nucleon potential is expected to be slightly repulsive [7–10]. Predictions have been made that the effective mass of the K^--meson decreases with increasing nuclear density leading to K^- condensation in neutron stars above 3 times the saturation density ρ_0. This effect is expected to influence significantly the evolution of supernova explosions: the K^- condensate softens the nuclear equation of state and thus causes a core with 1.5–2 solar masses to collapse into a black hole rather than to form a neutron star [11,12].

Heavy-ion collisions at relativistic energies — where baryonic densities of several times the saturation density are reached — offer the possibility to study in-medium properties of strange mesons. In dense nuclear matter the K^- effective mass is predicted to be reduced and thus the kinematical threshold for the process NN→K^-K^+NN will be lowered. As a consequence, the K^- yield in nucleus-nucleus collisions at bombarding energies below the NN threshold ($E_{\rm beam} = 2.5$ GeV for NN→K^+K^-NN) is expected to be enhanced significantly as compared to the

[a] e-mail: p.senger@gsi.de

case without in-medium mass reduction. In contrast, the yield of K^+-mesons is predicted to be decreased as the K^+ effective mass and thus the in-medium K^+ production threshold is slightly increased [13,14,9].

The large antikaon/kaon ratio measured in nucleus-nucleus collisions at "subthreshold" beam energies has been interpreted as a signature for significant in-medium modifications of antikaons [13–16]. Moreover, anisotropies of the azimuthal emission pattern of kaons have been measured and explained by an in-medium kaon nucleon potential [17,18]. The same explanation was proposed for the observation of a vanishing in-plane flow of kaons [19,20].

The various ratios of particles produced in nucleus-nucleus collisions can be used as a "thermometer" if an equilibrated fireball has been created [21,22]. Whether this happens or not is still a matter of debate. Up to now, particle ratios measured in Ni+Ni and Au+Au at SIS energies have been explained both by transport calculations and by a thermal model which assumes a common freeze-out temperature [22].

In contrast to heavy-collision systems, very light or strongly asymmetric systems allow to differentiate between theoretical descriptions such as thermal models or transport models. Predictions of statistical models — which are based on the assumption of a hadronic fireball in thermal and chemical equilibrium — might disagree with the data whereas transport models should be well suited for the description of nonequilibrated systems. Moreover, compressional effects are negligible in light symmetric collision systems, and hence nearly no collective flow is created. Therefore, the particle spectra reflect only the "thermal" energy of the particles. In addition, absorption effects should be small.

Another important aspect of particle production in nucleus-nucleus collisions is the absorption of particles in the cold spectator matter or in the dilute stage of the collision. This question is crucial when particle multiplicities are used as a "calorimeter" (to determine the thermal energy of a fireball) or as a probe for in-medium effects (*e.g.*, when particle yields or ratios are related to effective masses in nuclear matter). This aspect can be studied in strongly asymmetric collisions where the large target spectator provides a source of particle absorption.

Therefore, the comparison of particle yields in light symmetric and strongly asymmetric collision systems may shed light on i) in-medium and absorption effects in the absence of compression and flow and on ii) the predictive power of statistical and nonequilibrium models. There is also an experimental challenge connected with the interpretation of data measured in asymmetric collisions. As the velocity of the particle emitting source is not known *a priori*, it is hard to disentangle the effects of the Lorentz-boost, the polar angle distribution and rescattering of particles from spectator matter. These effects will be discussed below.

Pioneering experiments on kaon production in nucleus-nucleus collisions have been performed with a single-arm spectrometer at the BEVALAC [23]. Those measurements made use of the highest possible beam energy of 2.1 AGeV in order to enhance the kaon-to-proton ratio. Antikaons have been measured in beam-line spectrometers at $\Theta_{\rm lab} = 0^\circ$ which have a small acceptance in solid angle and momentum but an efficient partice identification capability [24,25]. In this article we present experimental results on the production of pions, kaons and antikaons in C+C and C+Au collisions at beam energies of 1.0 and 1.8 AGeV measured at various laboratory angles. The paper is arranged as follows. In the next chapter the experimental setup is described. Then the experimental results are presented: double-differential cross-sections for the production of pions, kaons and antikaons in the laboratory frame for C+C and C+Au collisions and invariant cross-sections for C+C collisions in the center-of-mass (c.m.) frame. For the symmetric system we find a nonisotropic polar angle distribution. Then we discuss the dependence of the particle multiplicities on the number of participating nucleons ($A_{\rm part}$) in symmetric collisions and use the scaling behaviour to estimate $A_{\rm part}$ for the asymmetric C+Au system. We determine the velocity of the particle emitting source in C+Au collisions with a transport calculation and discuss spectral shapes in the source frame. Finally we discuss in-medium effects and compare the data to the predictions of transport calculations.

2 Experimental setup

The experiments reported here have been performed with the Kaon Spectrometer (KaoS) [26] at the heavy-ion synchrotron SIS at GSI in Darmstadt. KaoS was designed to identify kaons and antikaons in collisions between heavy nuclei at very low beam energies: the proton/pion/kaon ratio can be as large as $10^6/10^4/1$. In order to make use of the highest beam intensities, the experiment is equipped with an efficient kaon trigger based on time-of-flight and Cherenkov detectors. Moreover, the KaoS setup is able to determine the centrality of the collision, the number of participants and the orientation of the reaction plane.

Figure 1 shows a sketch of the experimental setup. The spectrometer consists of a double-focussing quadrupole-dipole combination with a large acceptance in momentum ($p_{\rm max}/p_{\rm min} \approx 2$) and solid angle ($\Omega \leq 35$ msr). The maximum dipole magnetic field is $B = 1.95$ T corresponding to a momentum of $p_{\rm max} = 1.6$ GeV/c for particles with charge one.

The spectrometer is equipped with plastic scintillator arrays for time-of-flight measurements. The start detector consists of 16 elements (length 220 mm, width 30 mm, thickness 4 mm) and is located between the quadrupole and the dipole magnet. The time resolution is about 320 ps FWHM. The stop detector consists of 30 elements (length 380 mm, width 37 mm, thickness 20 mm) and is positioned along the focal plane of the spectrometer. The time resolution is about 100 ps FWHM, the distance from start to stop detector is 3–4 m depending on trajectory.

A plastic scintillator hodoscope (Large Angle Hodoscope, "LAH") consisting of 84 modules is located 8–13 cm downstream of the target. The modules are arranged in 3 rings and cover a polar angle range of $12^\circ < \Theta_{\rm lab} < 48^\circ$.

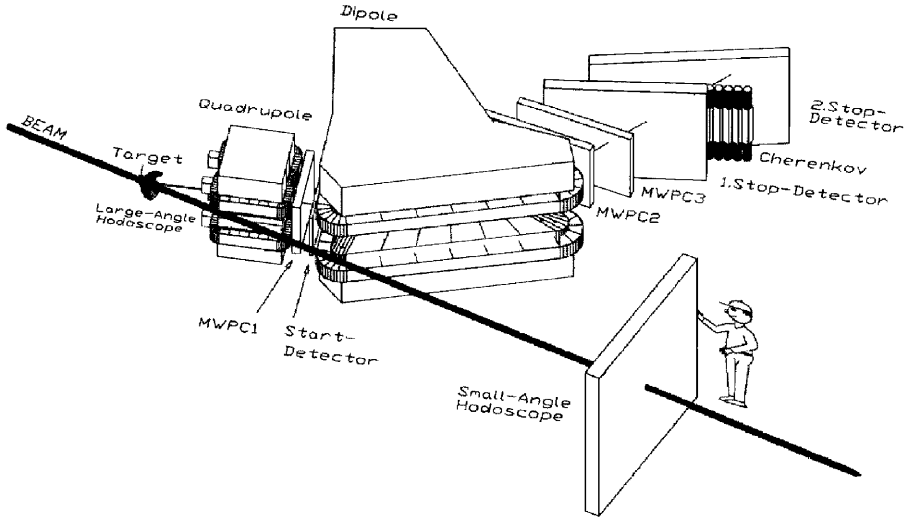

Fig. 1. Sketch of the Kaon Spectrometer and its detector system.

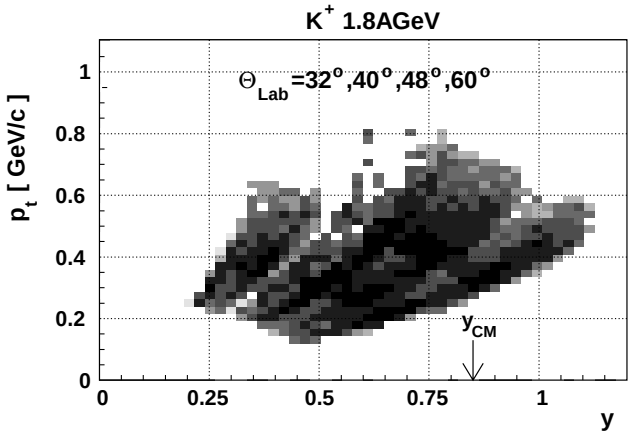

Fig. 2. Phase space covered by the Kaon Spectrometer with 4 angles and 3 magnetic fields in the transverse-momentum *vs.* rapidity plane. The scatter plot of the measured kaons is not corrected for acceptance.

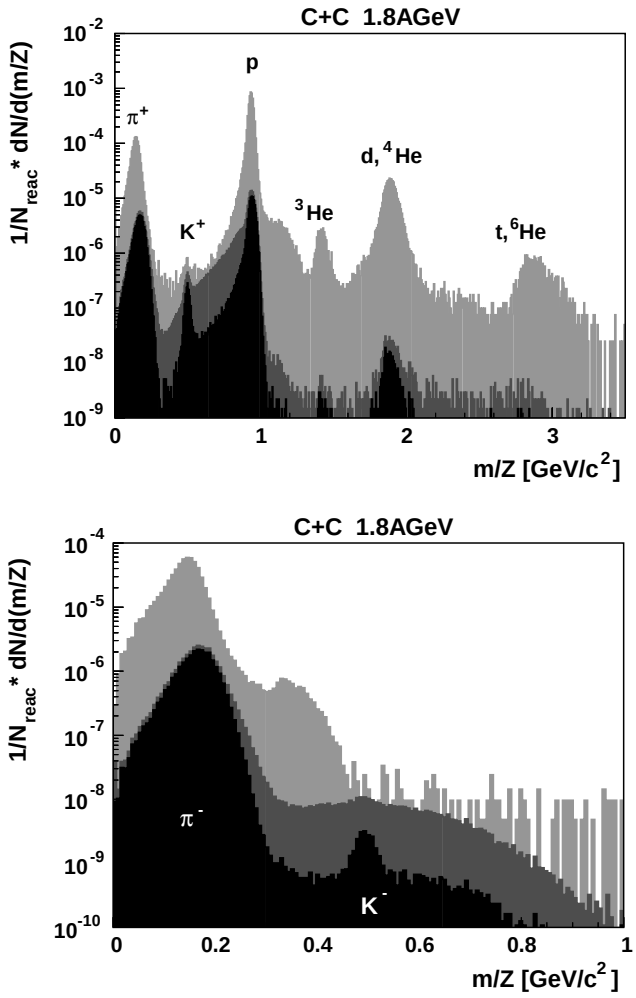

Fig. 3. Mass/Z distribution of positively (top) and negatively (bottom) charged particles for different trigger and tracking conditions.

This detector measures the multiplicity of charged particles which is correlated to the centrality of the collision. The time signals generated by the particles (mostly protons, deuterons and pions) in the LAH are used to determine the time when the reaction takes place in the target ($t = 0$). The time-of-flight between LAH and the start detector (distance about 1.7 m) provides additional independent information on the particle velocity. The comparison of the two measurements of the particle velocity (LAH-Start and Start-Stop) efficiently reduces the background of rescattered particles with false trajectories.

The particle trajectories were measured with three large area multiwire proportional chambers (MWPC). The first MWPC has an active area of 30×60 cm^2 and is located between quadrupole and dipole. The 2. and 3. MWPC have active areas of 35×120 cm^2 and are positioned between dipole magnet and stop detector. The position resolution of the chambers is 1 mm FWHM. The

quality of track recognition and vertex reconstruction is limited by small-angle straggling in the detectors and in the air.

A Cherenkov threshold detector is positioned behind the TOF stop wall [27]. The aim of this detector is to prevent high-energy protons from triggering the data aquisition, if the time-of-flight difference of protons and kaons is too small to be discriminated by the TOF trigger. The threshold velocity for particles producing Cherenkov light is $\beta = 1/n$ with n the refractive index of the radiator material. We chose lucite ($n = 1.49$) and water ($n = 1.34$) as radiators corresponding to threshold velocities of $\beta = 0.67$ and $\beta = 0.75$, respectively. The Cherenkov detector covers an area of 40×190 cm^2 and consists of 10 lucite modules at the low momentum side (height 40 cm, width 10 cm, thickness 5 cm) and 6 water modules at the high momentum side (height 40 cm, width 10 cm, thickness 10 cm). The overall efficiency of the Cherenkov detector for pions, kaons and protons is 0.96, 0.86 and 0.02, respectively, at particle momenta between 0.64 and 1.14 GeV/c.

The (hardware) kaon trigger is based on TOF and Cherenkov information. The kaon TOF trigger rejects all particles which differ in time-of-flight by a few nanoseconds from the nominal value of the kaon time-of-flight for a given magnetic field configuration. Depending on the magnetic field of the spectrometer, the kaon TOF trigger reduces the proton trigger rate by a factor of 10–100 and the pion trigger rate by a factor of about 10. At high magnetic fields where the TOF difference between protons and kaons becomes small, the requirement of a Cherenkov signal reduces the proton trigger rate by another factor of about 10 (with the TOF trigger active).

The spectrometer can be pivoted on the target point within the angular range of $0° < \Theta_{\rm lab} < 130°$. Figure 2 displays as an example the coverage of phase space achieved with 4 angles and 3 magnetic fields for kaons measured at 1.8 AGeV beam energy.

The beam intensity is determined with two plastic scintillator telescopes which consist of 3 detectors (40×40 mm^2) each. The telescope arms point to the target at $\Theta_{\rm lab} = 100°$ in the horizontal plane. The distance between the target and the first detector and between the subsequent detectors is 15 cm. The counting rate of the threefold coincidences of the detectors of each telescope arm is recorded with a scaler. This counting rate is proportional to the beam current. In fact, we take the average counting rate of the two telescopes in order to correct for a (horizontally) noncentral beam position at the target. The calibration factor (beam intensity/telescope counting rate) is determined by reducing the beam intensity to about 50000 ions/s and counting the beam directly with a movable plastic scintillator (20×20×3mm^3).

The challenge of the experiment is the identification of kaons and antikaons in the presence of a large background. This background is caused by i) rescattered particles, mostly high-energetic protons which hit the yoke of the quadrupole and are deflected into the focal plane detectors and ii) two particles from different reactions producing a random coincidence in the start/stop detectors and spurious tracks in the MWPCs. The reconstruction of these false tracks may result in an entry at a mass around 500 MeV/c^2 which contributes to the "background" below the kaon mass peak. Track recognition is performed by measuring hits in the second and third MWPC. These tracks are extrapolated to the first MWPC in which the calculated hit positions are compared to the measured ones. The calculation of the trajectories is based on GEANT simulations. Moreover, the tracks are extrapolated to the start and stop detectors and the calculated positions are compared to those paddles which had been hit by particles. Finally, the particle velocity measured between the LAH and the start detector is compared to the one measured between the start and the stop detector. A track is rejected, if the difference Δx (between measured and calculated positions) and the velocity difference $\Delta\beta$ (measured with the two TOF sections) exceed a value of 3 σ of the Δx and $\Delta\beta$ distributions, respectively. The losses due to these cuts are determined by kaon data with low background, *i.e.* kaon measurements at high bombarding energies (1.8–2.0 AGeV). These cuts are used also for the analysis of antikaons. The sum of all losses is about 20%.

The geometrical acceptance of the spectrometer and kaon decay in flight is determined by Monte Carlo simulations using the code GEANT. The kaon trigger efficiency is measured with the so-called "pseudokaons" which are protons (or pions) having the same velocity as the kaons in the experiment. This is achieved by choosing appropriate magnetic fields of dipole and quadrupole and using the same TOF-trigger conditions as for the kaon measurement. Similarly, the efficiency of the Cherenkov trigger is determined. The kaon trigger efficiency is about 90%. The efficiency of the MWPCs for the identification of minimum ionizing particles is measured to be better than 95%.

The quality of particle identification in C+C collisions at 1.8 AGeV is shown in fig. 3 for positively (top) and negatively charged particles (bottom) as function of their mass over charge ratio m/Z. The light grey spectrum is measured with a trigger on charged particles in the spectrometer without time-of-flight condition. The medium grey spectrum is measured with the TOF trigger. The dark spectrum is measured with the kaon trigger and analysed with conditions on tracking and particle velocity. The background near to the K mass is reduced by more than two orders of magnitude. What remains is quantified by a fit and is subtracted.

The measurements reported here have been performed with a carbon beam. The beam energy, the target isotope and thickness, the measured kaon rates and numbers are listed in table 1.

3 Experimental results

The systematic errors of the measured cross-sections presented in this chapter amount to about 15%. These errors are due to the uncertainties of beam normalization (7%), efficiencies of the TOF-trigger (5%), detector efficiencies (2%), track recognition (7%), kaon background subtrac-

Table 1. Beam energy, target isotope and thickness; approximate rates and total numbers of identified kaons and antikaons. The beam intensity is 10^8 ions per spill which had an average length of 4 s with a pause of 2 s (at 1 AGeV) and 4 s at (1.8 AGeV). The pion recording rate is typically 1–2×10^5/h.

Beam energy	Target	Target thickness	K^+ rate	K^- rate	K^+ number	K^- number
1.0 AGeV	^{12}C	5 mm	25/h	–	1200	–
1.8 AGeV	^{12}C	5 mm	900/h	25/h	17000	2000
1.0 AGeV	^{197}Au	0.5 mm	120/h	–	770	–
1.8 AGeV	^{197}Au	0.5 mm	3000/h	70/h	13000	1300

Table 2. System, beam energy, laboratory angles, inverse slope parameters, inclusive production cross-sections and multiplicities per participating nucleon for pions, kaons and antikaons. The values for T and σ are determined by fitting a Boltzmann distribution $\mathrm{d}^3\sigma/\mathrm{d}p^3 \propto \exp(-E/T)$ to the data. In the case of pions a superposition of two Boltzmann distributions is fitted and the slope parameter of the high-energy pions (T_2) quoted. In the extrapolation to full phase space the nonisotropic angular distribution is taken into account (see text). The definition of $M/\langle A_{\mathrm{part}}\rangle$ is given in the text. The quoted errors on the cross-sections include systematic effects.

System	Beam energy (AGeV)	Θ_{lab}	$T_2(\pi^+)$ (MeV)	$T(K^+)$ (MeV)	$\sigma(\pi^+)$ (b)	$\sigma(K^+)$ (mb)	$\frac{M(\pi^+)}{\langle A_{\mathrm{part}}\rangle}$ $\times10^{-2}$	$\frac{M(K^+)}{\langle A_{\mathrm{part}}\rangle}$ $\times10^{-5}$
C+C	1.0	44°, 70°	57±5	58±6	0.35±0.05	0.1±0.02	6.1±0.9	1.8±0.35
C+Au	1.0	44°, 70°	68±5	76±5	1.2±0.2	1.2±0.2	1.8±0.3	1.8±0.3
C+C	1.8	32°, 40°, 48°, 60°	76±5	75±5	0.69±0.1	3.0±0.3	12.1±1.8	53±5
C+Au	1.8	40°, 60°	80±6	90±6	5.0±0.7	30±5	7.6±1	45±8
System	Beam energy (AGeV)	Θ_{lab}	$T_2(\pi^-)$ (MeV)	$T(K^-)$ (MeV)	$\sigma(\pi^-)$ (b)	$\sigma(K^-)$ (mb)	$\frac{M(\pi^-)}{\langle A_{\mathrm{part}}\rangle}$ $\times10^{-2}$	$\frac{M(K^-)}{\langle A_{\mathrm{part}}\rangle}$ $\times10^{-5}$
C+C	1.8	40°, 60°	76±6	55±6	0.64±0.1	0.076±0.02	11.2±1.8	1.3±0.35
C+Au	1.8	40°, 60°	82±6	73±7	6.0±1	0.5±0.15	9.1±1.5	0.75±0.23

tion (5%), dead-time correction (7%) and acceptance calculation by GEANT (5%).

3.1 Differential production cross-sections

Figures 4 and 5 present the double differential cross-sections for the production of pions, kaons and antikaons in C+C and C+Au collisions at a beam energy of 1 AGeV and 1.8 AGeV, as function of the laboratory momentum. Each particle species has been measured at least at two laboratory angles in order to obtain an estimate of the polar angle distribution.

In order to study the properties of the particle emitting source, one has to determine the shape of the particle spectra and the angular distributions in its particular Lorentz frame. The transformation of the data into the center-of-mass of the participating nucleons is well defined only for symmetric systems. Therefore, we present in the following only the data taken in C+C collisions. The determination of the velocity of the particle emitting source in C+Au collisions will be discussed in the next chapter.

Figure 6 shows the invariant production cross-sections $E\,\mathrm{d}^3\sigma/\mathrm{d}p^3$ for pions, kaons and antikaons in C+C collisions at 1.0 (top) and 1.8 AGeV (bottom) as a function of their kinetic energy in the c.m. system. Boltzmann distributions $\mathrm{d}^3\sigma/\mathrm{d}p^3 \propto \exp(-E/T)$ have been fitted to the K^+ and K^- spectra. In contrast, the pion spectra cannot be described well by a single Boltzmann distribution. Therefore, a superposition of two distributions has been fitted to the pion differential cross-sections. The inverse slope parameters for the K-mesons and for the high energy pions are listed in table 2.

The K^+ (and K^-) spectra measured at different laboratory angles are slightly different when presented in the c.m. system. This indicates that the polar angle distribution is nonisotropic. A method to extract information on the angular distribution from our data is discussed in the next section.

3.2 Polar angle distributions in C + C collisions

In C+C collisions at 1.8 AGeV we have measured K^+-mesons at laboratory angles of $\Theta_{\mathrm{lab}} = 32°, 40°, 48°$ and 60°. Figure 7 shows the double differential cross-sections as function of the laboratory momentum. The dotted lines correspond to a simultaneous fit of a Boltzmann distribution $\mathrm{d}^3\sigma/\mathrm{d}p^3 \propto \exp(-E/T)$ to the spectra assuming isotropic emission. The fit results deviate systematically from the data: near midrapidity ($\Theta_{\mathrm{lab}} = 32°$) the fit overestimates the data whereas at backward rapidities

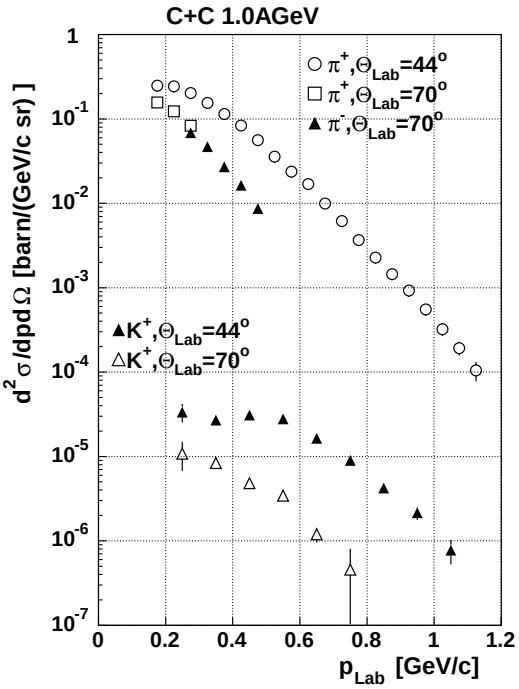

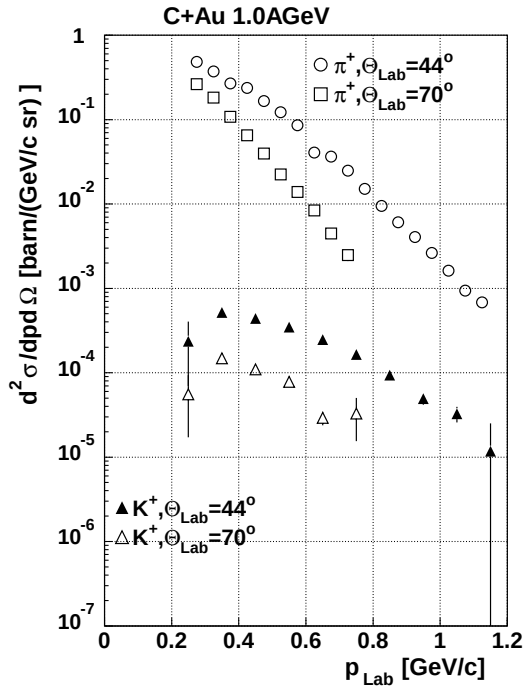

Fig. 4. Inclusive double-differential cross-sections for the production of pions and K^+-mesons measured in C+C (top) and C+Au (bottom) collisions at a beam energy of 1.0 AGeV under different laboratory angles (as indicated) as a function of laboratory momentum.

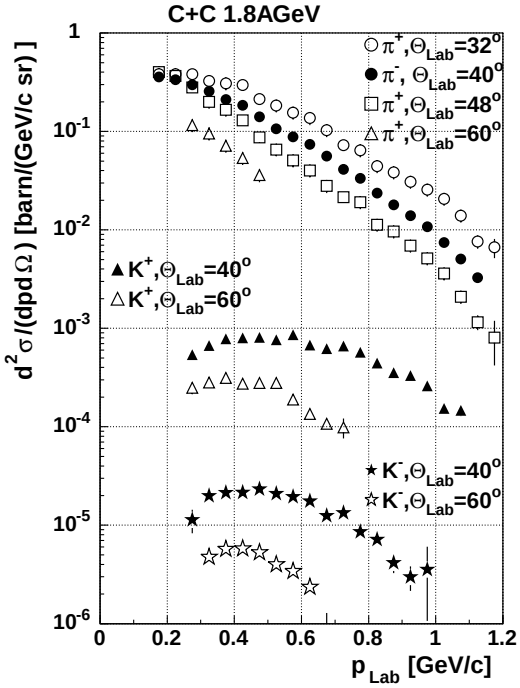

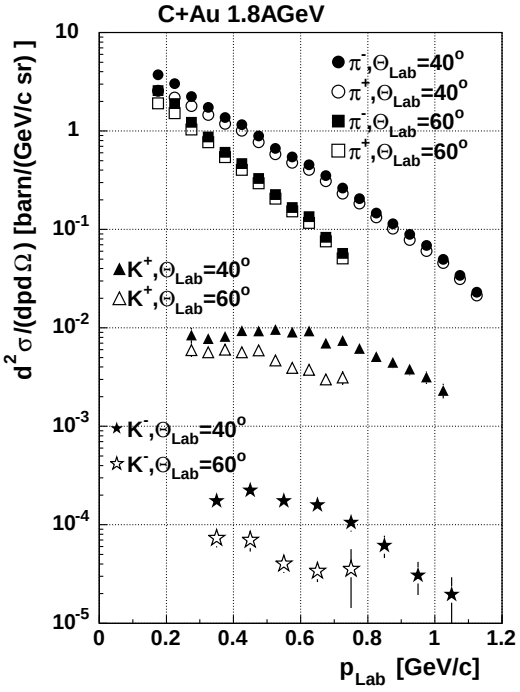

Fig. 5. Inclusive double-differential cross-sections for the production of pions, K^+-mesons and K^--mesons measured in C+C (top) and C+Au (bottom) collisions at a beam energy of 1.8 AGeV under different laboratory angles (as indicated) as a function of laboratory momentum.

($\Theta_{\rm lab} = 60°$) the fit underestimates the data. In order to improve the agreement between fit and data, we assume a forward-backward peaked polar-angle distribution according to

$$\mathrm{d}^3\sigma/\mathrm{d}p^3 \propto (1 + a_2 \cos^2 \Theta_{\rm c.m.}) \exp(-E/T)\,. \qquad (1)$$

The solid lines represent a simultaneous fit of this function to the data. The resulting parameters are $a_2 = 0.54 \pm 0.25$ and $T = 75 \pm 5$ MeV corresponding to a forward/backward peaked polar angle distribution. The fraction of nonisotropically emitted kaons can be determined

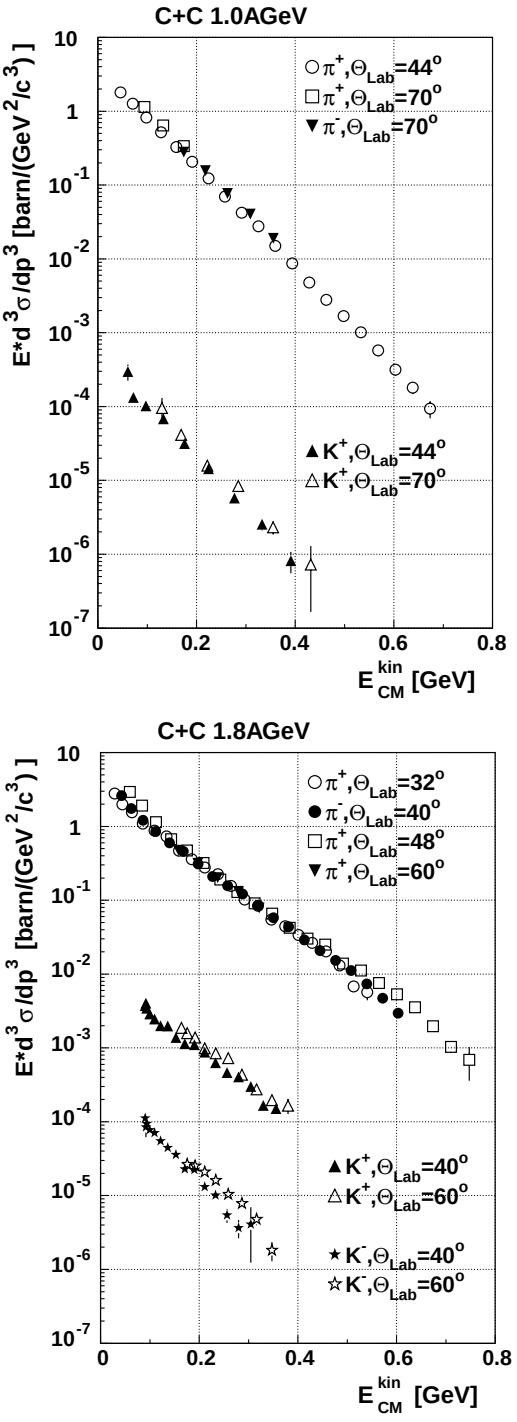

Fig. 6. Inclusive invariant cross-sections for the production of pions, K^+-mesons and K^--mesons measured in C+C collisions at a beam energy of 1.0 AGeV (top) and 1.8 AGeV (bottom) under different laboratory angles (as indicated) as a function of the c.m kinetic energy.

by integrating eq. (1) over full phase space:

$$\int \mathrm{d}p^3 \mathrm{d}^3\sigma/\mathrm{d}p^3 \propto$$
$$\int \mathrm{d}\phi\, \mathrm{d}\cos\Theta(1 + a_2\cos^2\Theta) \int p^2 \mathrm{d}p \exp(-E/T)\,, \quad (2)$$

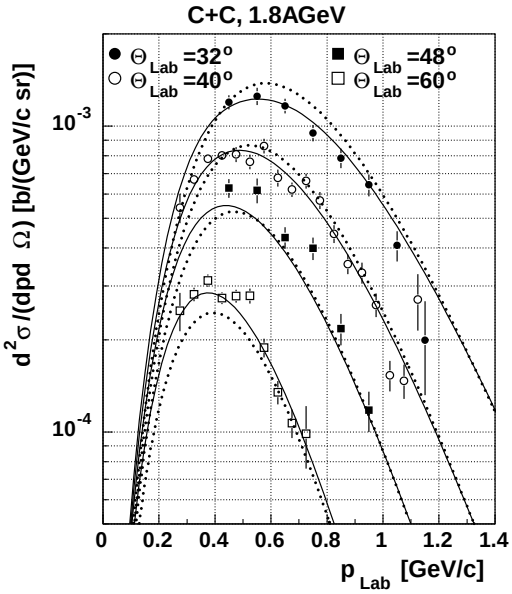

Fig. 7. Inclusive double-differential cross-sections for the production of K^+-mesons in C+C collisions at a beam energy of 1.8 AGeV under different laboratory angles (as indicated) as a function of the laboratory momentum. The lines represent a simultaneous fit of a Boltzmann distribution to the data assuming an isotropic (dotted lines) and a nonisotropic (solid lines) polar-angle distribution (see text).

with $\mathrm{d}p^3 = p^2 \mathrm{d}p\, \mathrm{d}\phi\, \mathrm{d}\cos\Theta$ and separation of the angular and momentum dependence. The integration over the angles yields $4\pi(1 + a_2/3)$. This means that the nonisotropic fraction of the total K^+ production cross-section is only $(a_2/3)/(1 + a_2/3) = 0.15 \pm 0.07$ for C+C collisions at 1.8 AGeV.

3.3 Total production cross-sections

When integrating the double-differential cross-sections for K^+ production in C+C collisions at 1.8 AGeV (as presented in fig. 7) over the full phase space assuming an isotropic emission in the c.m. system, one obtains for the total cross-section the values $\sigma_{K^+} = 2.4 \pm 0.3\,\mathrm{mb}(\Theta_{\mathrm{lab}} = 32°)$, $\sigma_{K^+} = 2.9 \pm 0.3\,\mathrm{mb}(\Theta_{\mathrm{lab}} = 40°)$, $\sigma_{K^+} = 3.3 \pm 0.3\,\mathrm{mb}(\Theta_{\mathrm{lab}} = 48°)$ and $\sigma_{K^+} = 3.6 \pm 0.4\,\mathrm{mb}(\Theta_{\mathrm{lab}} = 60°)$. The different results demonstrate the influence of the polar-angle distribution.

Total meson production cross-sections can be extracted from our data by integrating the fit function in eq. (1) over full phase space. Using this procedure we obtain for the total K^+ production cross-section in C+C collisions at 1.8 AGeV a value of $\sigma_{K^+} = 3.0 \pm 0.3$ mb.

A second method for the determination of the production cross-section is based on i) the assumption of a parabolic polar angle distribution (according to eq. (1)) and on ii) the observation that for a certain laboratory angle an isotropic particle source and a nonisotropic source yield the same differential cross-section. This matching angle is about $\Theta_{\mathrm{lab}} = 42°$ for K^+-mesons from C+C pro-

duction at 1.8 AGeV (see fig. 7). Therefore, the total cross-sections calculated for different laboratory angles (assuming isotropic emission, see above) can be interpolated to the angle of $\Theta_{\rm lab} = 42°$. The result is $\sigma_{\rm K^+} = 3.0\pm0.3$ mb, exactly the same value as for the simultaneous fit of a nonisotropic angular distribution. The second method has the advantage that the result of the interpolation is largely independent of the value of a_2. Therefore, the error of a_2 which might be very large when only two laboratory angles have been measured, influences the result only weakly. The matching angle depends only on the beam energy and on the assumption of a parabolic polar angle distribution.

Table 2 contains the total production cross-sections for pions, kaons and antikaons measured in C+C and C+Au collisions at 1.0 and 1.8 AGeV. The calculation of the cross-sections for the asymmetric C+Au system requires information on the velocity of the particle emitting source (see next section).

3.4 The kaon-emitting source in C + Au collisions

In order to study the properties of the fireball the particle observables have to be analysed in the rest frame of the source. For a symmetric collision system, this frame coincides with the center-of-mass frame of the nuclei (*i.e.* the nucleon-nucleon c.m. frame). For the asymmetric C+Au system the situation is much less clear. In a first step, one can roughly estimate the number of the participating nucleons (and their origin) for the C+Au system by a geometrical model assuming straight line geometry [28]

$$\langle A_{\rm part}\rangle = \frac{A_{\rm P}\pi R_{\rm T}^2 + A_{\rm T}\pi R_{\rm P}^2}{\pi(R_{\rm P}+R_{\rm T})^2}\,, \qquad (3)$$

with $A_{\rm P}$ and $A_{\rm T}$ the mass number and $R_{\rm P}$ and $R_{\rm T}$ the radius of projectile and target nucleus, respectively. For symmetric collisions systems the average number of participants is $\langle A_{\rm part}\rangle = A/2$, *i.e.* $\langle A_{\rm part}\rangle = 6$ for ^{12}C+^{12}C collisions. For ^{12}C+^{197}Au collisions the average number of participants (for inclusive reactions) is $\langle A_{\rm part}\rangle = 22$ with 6.6 participants from the projectile and 15.4 from the target nucleus according to eq. (3).

However, with respect to particle production, the number of participating nucleons from the target nucleus might differ from the geometrical estimate. Therefore, we have extracted the velocity of the particle-emitting source from a transport model calculation. Bratkowskaya and Cassing have calculated K^+ production in C+Au collisions at 1.8 AGeV with their RBUU code [2] and made the events available to us. The calculation uses a parameterization of elementary cross-sections which is based on data including those recently measured at COSY [29] and takes into account rescattering and in-medium effects. The predictions of the model calculation agree well with the differential cross-sections for K^+ and K^- production in C+C and C+Au collisions (see sect. 4). We have analysed the momentum distribution of the kaons and have determined the reference frame in which the average longitudinal momentum of the kaons is zero. This frame moves with the velocity of a fireball which contains twice as many nucleons from the target than from the projectile nucleus (*e.g.* 6 projectile nucleons and 12 target nucleons). The fireball velocity is $\beta = 0.44$ for the C+Au system at 1 AGeV (as compared to $\beta = 0.59$ for C+C at 1 AGeV) and $\beta = 0.56$ for the C+Au system at 1.8 AGeV (as compared to $\beta = 0.70$ for C+C).

Within these source frames both kaons and antikaons are emitted nearly isotropically. This is demonstrated for K^+-mesons in the upper part of fig. 8 both for RBUU predictions and data. Figure 8 (top) presents the invariant cross-sections for K^+ production in C+Au collisions at 1.8 AGeV transformed into the frame of the source which contains twice as much nucleons from the target nucleus than from the projectile. The K^+ spectra taken at $\Theta_{\rm lab} = 40°$ and 60° nearly coincide in this representation. In contrast, when transforming measured and calculated spectra into the nucleon-nucleon frame (*e.g.*, a source containing 6 nucleons from the projectile and 6 from the target) the polar angle distribution appears very much nonisotropic (see lower part of fig. 8).

In order to determine spectral distributions and multiplicities of pions, kaons and antikaons from C+Au collisions, we adopt source velocities of $\beta = 0.45$ and 0.56 for beam energies of 1.0 and 1.8 AGeV, respectively, as given by the RBUU transport calculation for K^+ and K^--mesons. Figure 9 presents the invariant meson production cross-sections in C+Au collisions at 1.0 AGeV (top) and 1.8 AGeV (bottom) as a function of the kinetic energy in the source frame. Boltzmann distributions have been fitted to the data (not shown in fig. 9). The resulting inverse slope parameters are given in table 2.

3.5 Particle multiplicities

Inclusive cross-sections for the production of pions, kaons and antikaons in C+Au collisions have been determined from fig. 9. The Boltzmann distributions are used to extrapolate over the non-measured regions of phase space taking into account the angular distributions as measured. The cross-sections are listed in table 2. The multiplicity of produced particles per collision can be calculated by $M = \sigma/\sigma_R$ with σ the production cross-section. The geometrical reaction cross-section for a collision of two nuclei with masses $A_{\rm P}$ and $A_{\rm T}$ is defined as

$$\sigma_R = \pi(r_0 A_{\rm P}^{1/3} + r_0 A_{\rm T}^{1/3})^2\,, \qquad (4)$$

with $r_0 = 1.2$ fm. This definition yields $\sigma_R = 0.95$ barns for the ^{12}C+^{12}C system and $\sigma_R = 3.0$ barns for ^{12}C+^{197}Au collisions. Table 2 includes the particle multiplicities per participating nucleon $M/\langle A_{\rm part}\rangle$. The average number of participating nucleons $\langle A_{\rm part}\rangle$ is calculated for inclusive reactions according to eq. 3.

It is interesting to note that the pion multiplicity per participating nucleon $M(\pi^+)/\langle A_{\rm part}\rangle$ is a factor of more than three smaller in C+Au than in C+C collisions at 1 AGeV (the effect of isospin might change this factor

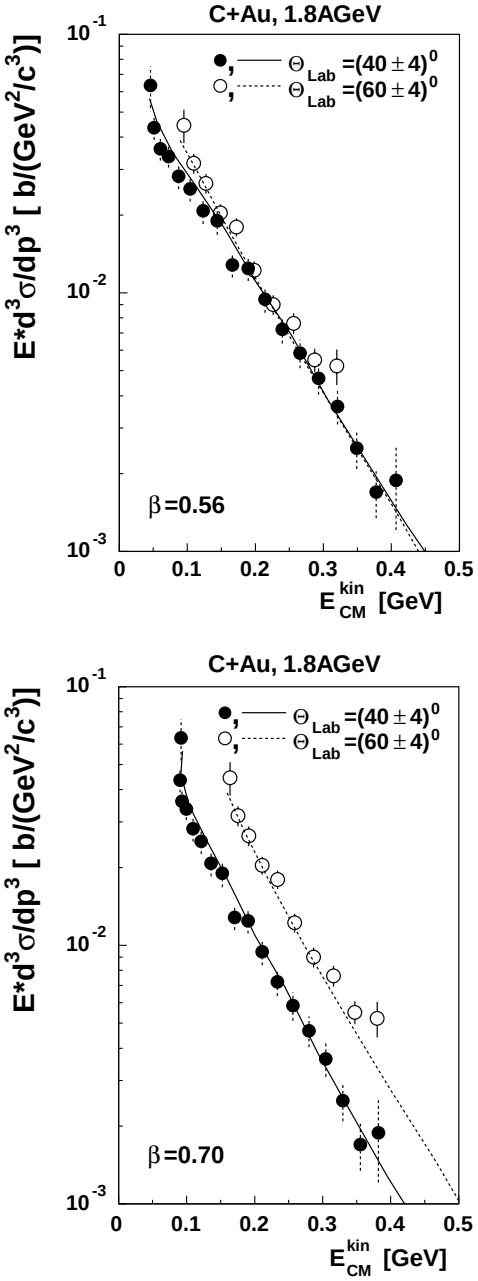

Fig. 8. Inclusive invariant cross-sections for the production of K^+-mesons measured in C+Au collisions at a beam energy of 1.8 AGeV as a function of the kinetic energy in different source frames. The source velocity is assumed to be either $\beta = 0.70$ (corresponding to the nucleon-nucleon system, bottom figure) or $\beta = 0.56$ (corresponding to a source which contains twice as much nucleons from the target nucleus than from the projectile, top figure) The data (full/open symbols) and the RBUU predictions (solid/dashed lines) are taken at $\Theta_{\rm lab} = 40^\circ/60^\circ$.

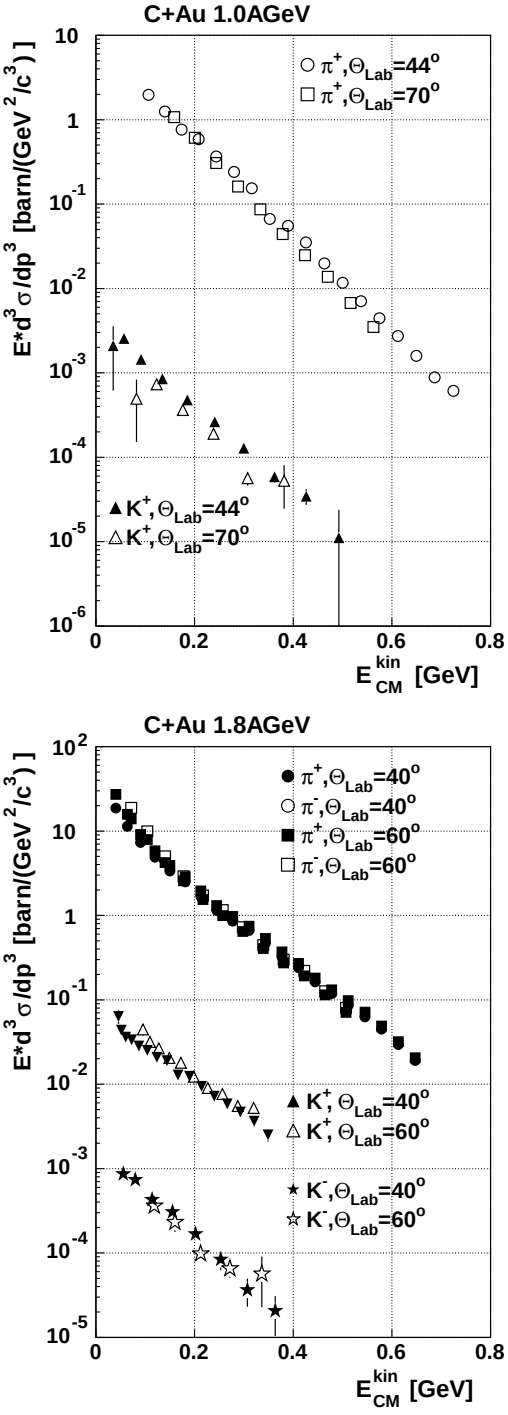

Fig. 9. Inclusive invariant cross-sections for the production of pions, K^+-mesons and K^--mesons measured in C+Au collisions at a beam energy of 1.0 AGeV (top) and 1.8 AGeV (bottom) as a function of the kinetic energy in the source frame. The source moves with the velocity of the center-of-mass of a system containing one projectile nucleon and two target nucleons.

slightly, in C+Au collisions at 1.8 AGeV the π^+/π^- ratio is 0.84±0.18). The TAPS Collaboration measured neutral pions in C+C and C+Au collisions at 0.8 AGeV (at midrapidity in the NN system) and found $M(\pi^0)/\langle A_{\rm part}\rangle$ reduced by a factor of about 2 when using the heavy target [30]. At a beam energy of 1.8 AGeV, however, the pion multiplicities per participating nucleon in C+C and C+Au collisions differ only by a factor of about 0.7 (averaged value for π^+ and π^-).

The strong reduction of the pion multiplicity per participant in C+Au collisions at 1 AGeV as compared to the C+C system indicates that pions are reabsorbed in the large gold nucleus. When increasing the projectile energy, the projectile nucleons will collide subsequently with nucleons in the Au target at energies well above the pion production threshold. This effect increases the number of produced pions and thus compensates partly for absorption. Such a scenario explains — at least qualitatively — the observation that the pion multiplicity per participating nucleon rises faster with beam energy in C+Au than in C+C collisions and hence is almost similar for both targets at a beam energy of 1.8 AGeV (see table 2).

In contrast to the pions, the values of the K^+ multiplicities per nucleon $M(K^+)/\langle A_{\rm part}\rangle$ are very similar for C+C and C+Au collisions at 1 AGeV and at 1.8 AGeV. From symmetric collision systems at beam energies below or near the K^+ production threshold, it is known that $M(K^+)$ increases more than linearly with $\langle A_{\rm part}\rangle$ [15,16]. The similar values of $M(K^+)/\langle A_{\rm part}\rangle$ for C+C and C+Au indicate that the energy per participating nucleon available for particle production in C+Au collisions is smaller than in the C+C system.

In Ni+Ni collisions at 1.8 AGeV it was found that the multiplicities of K^- and K^+ mesons scale similarly with $\langle A_{\rm part}\rangle$ [15]. Therefore, one would expect also an enhancement of $M(K^-)/\langle A_{\rm part}\rangle$ for C+Au as compared to C+C collisions at 1.8 AGeV. However, we observe that the K^- multiplicity per participating nucleon is reduced by a factor of 0.55 in the C+Au system. This result indicates a significant loss of K^--mesons in C+Au collisions which overcompensates for the expected enhancement. The loss may be caused by reabsorption of antikaons in the heavy target nucleus via the strangeness exchange reaction $K^-N \rightarrow \Lambda\pi$. The inelastic K^-p cross-section (at K^- momenta of 300 MeV/c) is about 40 mb [31]. This corresponds to a mean free path of about $\lambda \approx 1.5$ fm for K^--mesons in nuclear matter at saturation density ($\rho_0 = 0.17$ fm^{-3}).

Our data indicate that the absorption of antikaons is an important process in nucleus-nucleus collisions. This effect has to be understood quantitatively if one tries to extract information on the in-medium properties of antikaons from heavy-ion data. In the small C+C collision system, however, K^- absorption should be of minor importance and in-medium effects might be observable.

A way to visualize the effect of the nuclear medium on the production of kaons and antikaons is proposed in fig. 10 (taken from [16]). The figure presents the K^+ and K^- multiplicities per participating nucleon for C+C and nucleon-nucleon collisions as a function of the energy

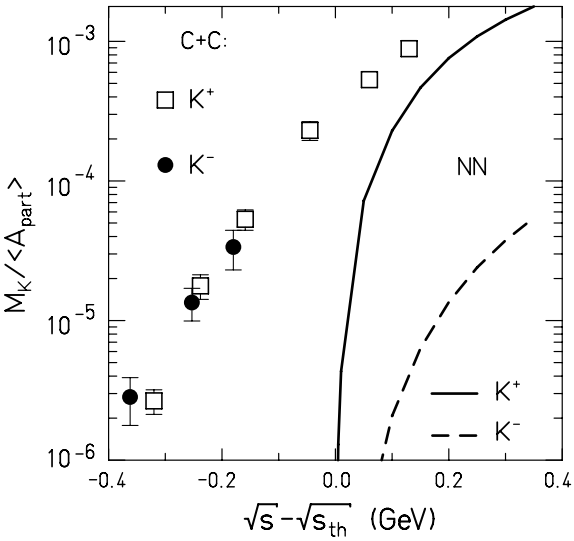

Fig. 10. Kaon and antikaon multiplicity per participating nucleon as a function of the Q-value for C+C collisions (open squares: K^+, full dots: K^-) and nucleon-nucleon collisions. The error bars include systematic effects. The lines (NN) correspond to parameterizations of the isospin averaged cross-sections for K-meson production measured in proton-proton collisions (full line: K^+, dashed line: K^-) [32–34].

above threshold ($\sqrt{s}-\sqrt{s}_{\rm th}$) in the nucleon-nucleon (NN) system. The values of the excess energy $\sqrt{s}-\sqrt{s}_{\rm th}$ are calculated according to $s = (E_{\rm pro} + 2m_{\rm N})^2 - p_{\rm pro}^2$, with $E_{\rm pro}$ and $p_{\rm pro}$ the projectile kinetic energy and momentum per nucleon and $m_{\rm N}$ the nucleon mass. The threshold energy is $\sqrt{s}_{\rm th} = m_{\rm K} + m_\Lambda + m_{\rm N} = 2.55\,{\rm GeV}$ for K^+ production and $\sqrt{s}_{\rm th} = 2m_{\rm K} + 2m_{\rm N} = 2.86\,{\rm GeV}$ for K^-K^+ pair production.

The solid and the dashed line in fig. 10 represent the parameterizations of the isospin-averaged cross-sections for K^+ and K^- production in nucleon-nucleon collisions [32–34]. These calculations reproduce the available experimental cross-sections including data measured recently close to threshold at COSY and SATURNE [29,35]. The multiplicities as shown in fig. 10 are calculated from the elementary cross-sections using $\sigma_R = 45$ mb and $A_{\rm part} = 2$ for nucleon-nucleon collisions.

The data in fig. 10 demonstrate that the excitation functions for K^+ and K^- production in C+C collisions are quite similar when correcting the energy axis for the threshold energies. In nucleon-nucleon (NN) collisions, however, the K^+ yield exceeds the K^- yield by 1–2 orders of magnitude for beam energies close to threshold. The comparison of the K^+ and K^- excitation functions for C+C and nucleon-nucleon reactions near threshold clearly indicates that in the nuclear medium the K^- multiplicity is much more enhanced than the K^+ multiplicity. Possible reasons for the enhancement of K^- production in nucleus-nucleus collisions will be discussed in the next section.

4 Medium effects in kaon and antikaon production

In nucleus-nucleus collisions at bombarding energies near the production threshold, strange mesons are created predominantly in secondary processes like $\pi N \rightarrow K^+Y$, $\Delta N \rightarrow K^+YN$, $\pi N \rightarrow K^-K^+N$, $\Delta N \rightarrow K^-K^+NN$ and $\pi Y \rightarrow K^-N$ with $Y = \Lambda, \Sigma$. These processes represent mechanisms of energy accumulation via multiple collisions. Moreover, the effective particle production threshold is lowered by the Fermi motion of the nucleons. Therefore, kaons and antikaons are observed in C+C collisions below the nucleon-nucleon threshold of $\sqrt{s} - \sqrt{s}_{\rm th} = 0$ (see fig. 10). According to relativistic transport models, the pion- and Δ-induced sequential processes dominate the K^+ production at bombarding energies near the kinematical threshold [13,36]. In the case of K^--mesons, however, the most important channel is expected to be the strangeness exchange reaction $\pi Y \rightarrow K^-N$. However, the calculations which take into account these secondary K^- production channels (including K^- absorption) underpredict the K^- yield measured in Ni+Ni collisions at 1.8 AGeV [15] by a factor of about 6 when neglecting in-medium mass modifications of K^--mesons [13].

4.1 K^+ and K^- production at equivalent beam energies

One would expect that density-dependent in-medium effects are more pronounced in Ni+Ni than in C+C collisions. As illustrated in fig. 10 medium effects can be quantified for example by the measured ratio K^-(1.8 AGeV)/K^+(1.0 AGeV). These two energies are "equivalent" in the sense that they correspond to very similar (negative) values for the excess energy of $\sqrt{s} - \sqrt{s}_{\rm th} \approx -0.23$ GeV. However, this ratio is 1±0.4 for Ni+Ni [15] and 0.76±0.25 for C+C [16], *i.e.* there is no difference within the error bars. On the other hand, the reabsorption of antikaons should be enhanced in larger systems. This effect may cancel the enhancement due to the in-medium effect with the consequence that the K^-/K^+ ratio at equivalent energies is independent of the size of the collision system.

Figure 11 presents the invariant production cross-sections of K^+ and K^--mesons as a function of c.m. kinetic energy for C+C (top) and C+Au (bottom) collisions at "equivalent" beam energies. In C+C collisions, the K^+ yield measured at 1.0 AGeV agrees to the K^- yield taken at 1.8 AGeV similar as for Ni+Ni. In C+Au collisions, however, the K^- data are reduced with respect to the K^+ data by more than a factor of 2. This observation may be explained by reabsorption of antikaons in the target spectator nucleus.

4.2 Comparison to transport model calculations

In the following we will compare the kaon and antikaon data to predictions of RBUU transport calculations [2].

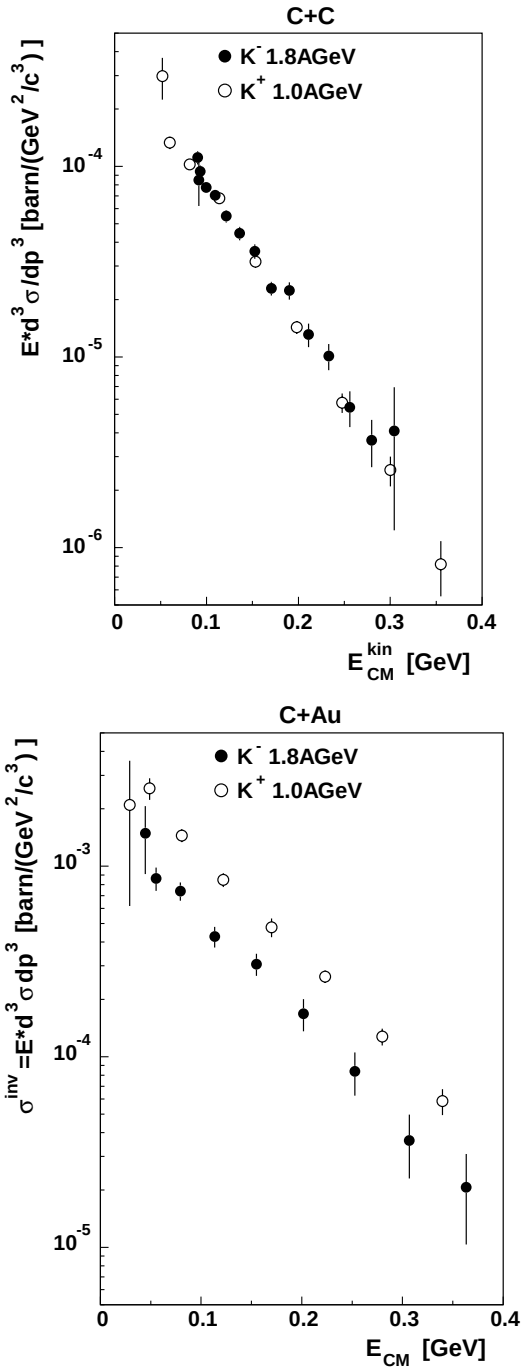

Fig. 11. Comparison of invariant cross-sections for K^- and K^+ production at equivalent energies (see text) in C+C (top) and C+Au collisions (bottom).

The model takes into account the in-medium modification of the effective masses of strange mesons according to $m^*_{\rm K} = m^0_{\rm K}\ (1 - a\rho/\rho_0)$, with $m^0_{\rm K}$ the kaon mass in the vacuum, ρ the baryonic density inside the reaction zone, ρ_0 the saturation density and $a = -0.06$ for kaons and $a = 0.24$ for antikaons. The values of a correspond to a slight increase of the kaon mass with increasing baryonic density (12% at $\rho = 2\rho_0$) and a significant decrease of the effective

antikaon mass (48% at $\rho = 2\rho_0$). The assumption on the linear density dependence of the kaon and antikaon masses reproduces a trend found by various calculations [8,9]. It should be mentioned that the effect of dynamical spectral functions on the in-medium properties of K-mesons [10] is ignored in this simple parameterization.

The variation of the effective masses changes the in-medium production thresholds and thus the kaon and antikaon yields. At beam energies below and near the thresholds, the kaon and antikaon excitation function rises steeply with increasing bombarding energy and thus the kaon and antikaon yields depend very sensitively upon the in-medium thresholds.

In fig. 12 and fig. 13 the measured kaon and antikaon invariant production cross-sections are compared to predictions of RBUU transport calculations [37]. The solid lines correspond to the result of the transport code if in-medium effects are taken into account. The dashed lines represent the calculation assuming "bare" masses. For C+C collisions at 1.0 AGeV (fig. 12, upper part) the kaon data clearly favor the "in-medium" calculation in contrast to the kaon data measured in the same system at 1.8 AGeV (fig. 13, lower part). In C+Au collisions both at 1.0 AGeV (fig. 12, lower part) and at 1.8 AGeV (fig. 13, lower part) the data cannot distinguish the two calculations. Hence, no clear signature of in-medium effects on K^+ production emerges from the comparison of RBUU calculations and experiment. However, transport calculations performed recently with two QMD codes [38] are able to reproduce K^+ production cross-sections measured in C+C collisions at bombarding energies between 0.8 and 2.0 AGeV only when taking account a repulsive KN potential.

On the other hand, the RBUU model calculation predicts an enhanced K^- yield when in-medium effects are taken into account (see fig. 13). For C+C collisions at 1.8 AGeV, the K^- differential cross-section exceeds the "bare mass" calculation by about a factor of 5 whereas the enhancement is less pronounced in C+Au collisions at 1.8 AGeV. Hence, the measured antikaon yield is much better (although not perfectly) described by the calculations with in-medium effects included.

As mentioned before, the measured cross-sections are affected by an uncertainty of 15% due to systematic errors. Moreover, the results of the model calculations depend in absolute yield on the treatment of momentum dependent interactions, the role of pions and baryonic resonances, the nuclear equation of state, etc. In order to reduce these uncertainties, we present in fig. 14 the K^-/K^+ ratios in C+C collisions (top) and C+Au collisions (bottom) at a beam energy of 1.8 AGeV as function of the c.m. kinetic energy. The calculations predict two important features of the data: the relative yields and spectral slopes of kaons and antikaons. According to the RBUU calculation, the steeper spectral slope of the antikaons with respect to the kaons is caused by the in-medium kaon-nucleon potentials which are repulsive for kaons but attractive for antikaons. The number of calculated antikaons is much smaller than the number of measured antikaons. Therefore, we have grouped the calculated K-mesons into 3–4 bins only. This presentation causes the discontinuities of the model results.

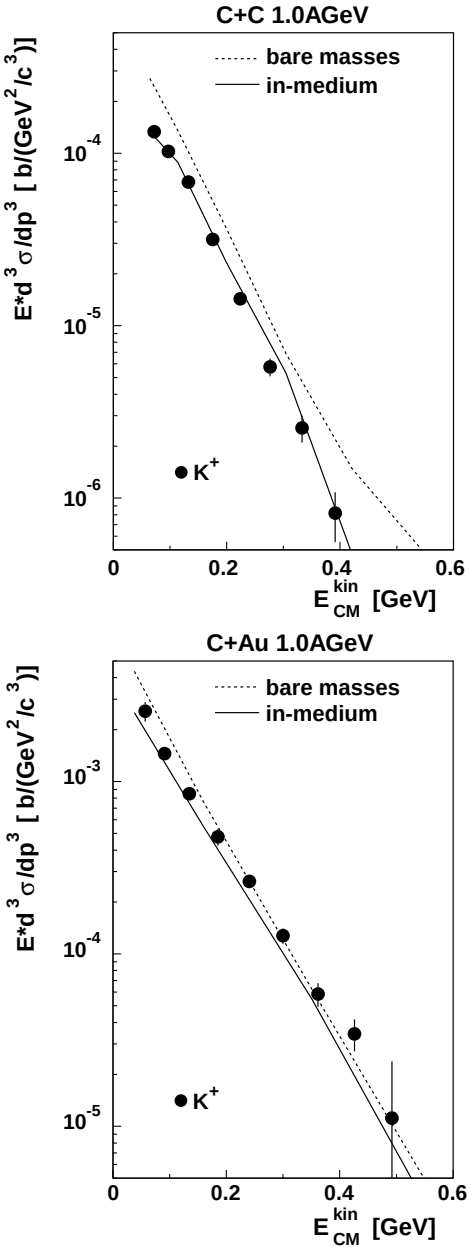

Fig. 12. Invariant cross-sections for K^+ production in C+C (top) and C+Au collisions (bottom) at 1.0 AGeV. The data are compared to results of a RBUU transport calculation with (solid lines) and without (dashed lines) in-medium modifications of the K^+-mesons [37].

5 Conclusions

We have presented production cross-sections of charged pions, kaons and antikaons measured in C+C and C+Au

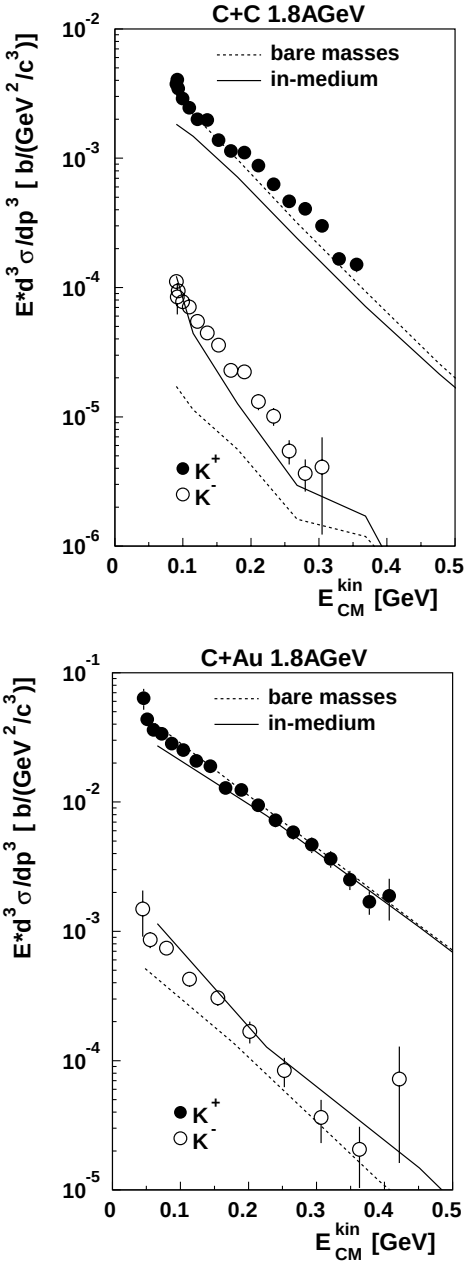

Fig. 13. Invariant cross-sections for K^+ and K^- production in C+C (top) and C+Au collisions (bottom) at 1.8 AGeV. The data are compared to results of a RBUU transport calculation with (solid lines) and without (dashed lines) in-medium modifications of the K-mesons [37].

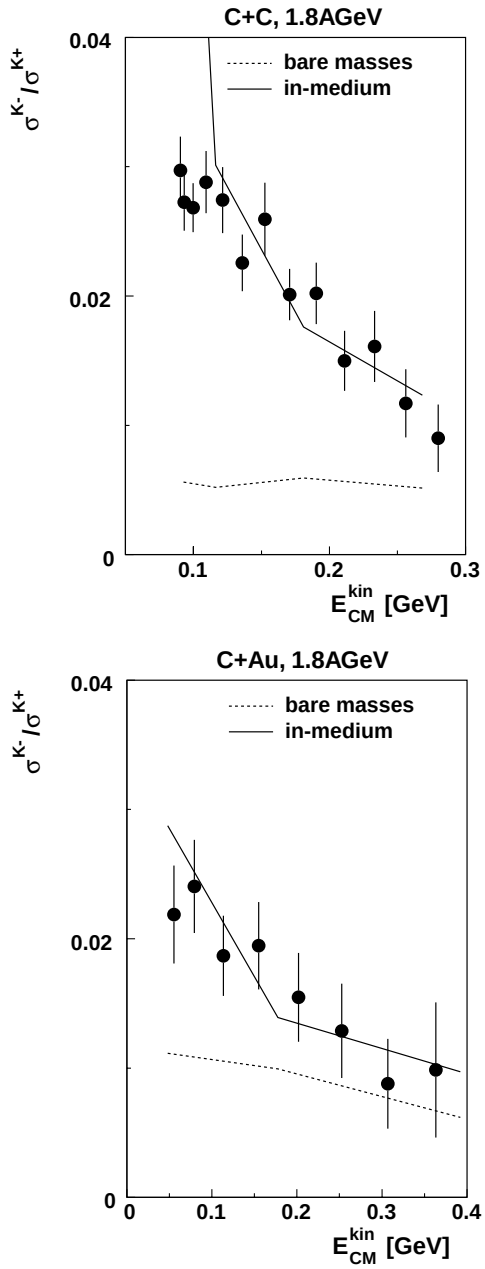

Fig. 14. K^-/K^+ ratio for C+C (top) and C+Au collisions (bottom) at 1.8 AGeV. The data are compared to results of a RBUU transport calculation without (solid lines) and with (dashed lines) in-medium modifications of the K-mesons [37]. The data shown in the top figure have been published in [16].

collisions at beam energies of 1.0 and 1.8 AGeV at different polar emission angles. For the asymmetric $^{12}C+^{197}Au$ system we have determined the velocity of the K-meson emitting source by transport calculations. It turns out that the source moves with the velocity of the center-of-mass of one nucleon from the projectile and two nucleons from the target. Within this frame both the calculated and the measured K-mesons exhibit essentially an isotropic emision pattern.

The kaon and antikaon spectra are described by Boltzmann distributions whereas the pion spectra exhibit an additional enhancement at low energies. The spectral slopes are similar for high-energy pions and kaons but are steeper for antikaons. The inverse slope parameters increase both with beam energy and target size.

At a beam energy of 1 AGeV, the pion multiplicity per participating nucleon $M(\pi^+)/\langle A_{\rm part}\rangle$ is about a factor of three smaller in C+Au than in C+C collisions whereas at

1.8 AGeV the values differ much less. The K^+ multiplicity per participating nucleon $M(K^+)/\langle A_{\rm part}\rangle$ is similar for C+C and C+Au collisions at 1 AGeV and at 1.8 AGeV. These observations indicate that in C+Au collisions at 1 AGeV the pions are reabsorbed in the large gold nucleus (this effect is not expected for K^+-mesons due to their antistrange quark content). At a beam energy of 1.8 AGeV, however, energetic secondary collisions of projectile nucleons with nucleons in the Au target may contribute to pion production thus compensating for losses due to reabsorption.

In contrast to the K^+-mesons, the K^- multiplicity per participating nucleon decreases by a factor of 0.55 in C+Au as compared to C+C collisions at 1.8 AGeV. This result indicates that K^--mesons are strongly absorbed by the heavy target nucleus. This effect would also explain that the K^-/K^+ ratios at equivalent energies are smaller for C+Au than for C+C collisions.

RBUU transport model calculations predict the K^+ data within a factor of two depending on the assumption on the in-medium effective mass of the K^+-mesons. For C+C collisions at 1 AGeV, the K^+ data favor the calculation based on the in-medium kaon mass whereas for C+C collisions at 1.8 AGeV the bare mass option is closer to the data. For C+Au collisions both assumptions on the K^+ effective in-medium mass explain the data equally well.

The yield of K^--mesons measured in C+C collisions at 1.8 AGeV is clearly underpredicted by the transport calculations if a bare antikaon mass is assumed. The agreement with the data is improved when assuming an attractive antikaon-nucleon potential in the nuclear medium. For C+Au collisions at 1.8 AGeV the data can hardly distinguish between the two options of the K^- in-medium effective mass. In this case the effect of the in-medium potential — which depends on the baryon density — may be washed out by the the strong absorption of K^- in the gold nucleus.

In summary, the RBUU transport calculations describe both kaon and antikaon data within a factor of about two with consistent assumptions on in-medium effects. The accuracy of the calculations has to be further improved in order to extract conclusive information on the in-medium properties of strange mesons.

We thank Elena Bratkowskaya and Wolfgang Cassing for providing us with the results of their transport calculations and for various discussions. This work was supported by the German Federal Government (BMBF), by the Polish Committee of Scientific Research (Contract No. 2P03B11515) and by the GSI fund for University collaborations.

References

1. R. Stock, Phys. Rep. **135**, 259 (1986).
2. W. Cassing, E. Bratkovskaya, Phys. Rep. **308**, 65 (1999).
3. P. Senger, H. Ströbele, J. Phys. G: Nucl. Part. Phys. **25** (1999). R59
4. J.W. Harris et al., Phys. Lett. B **153**, 377 (1985).
5. J. Aichelin, C.M. Ko, Phys. Rev. Lett. **55**, 2661 (1985).
6. G.Q. Li, C.M. Ko, Phys. Lett. B **349**, 405 (1995).
7. G.E. Brown, C.H. Lee, M. Rho, V. Thorsson, Nucl. Phys. A **567**, 937 (1994).
8. T. Waas, N. Kaiser, W. Weise, Phys. Lett. B **379**, 34 (1996).
9. J. Schaffner-Bielich, J. Bondorf, I. Mishustin, Nucl. Phys. A **625**, 325 (1997).
10. M. Lutz, Phys. Lett. B **426**, 12 (1998).
11. G.E. Brown, H.A. Bethe, Astrophys. J. **423**, 659 (1994).
12. G.Q. Li, C.H. Lee, G.E. Brown, Phys. Rev. Lett. **79**, 5214 (1997).
13. W. Cassing et al., Nucl. Phys. A **614**, 415 (1997).
14. G.Q. Li, C.M. Ko, X.S. Fang, Phys. Lett. B **329**, 149 (1994).
15. R. Barth et al., Phys. Rev. Lett. **78**, 4007 (1997).
16. F. Laue et al., Phys. Rev. Lett. **82**, 1640 (1999).
17. Y. Shin et al., Phys. Rev. Lett. **81**, 1576 (1998).
18. G.Q. Li, C.M. Ko and G.E. Brown, Phys. Lett. B **381**, 17 (1996).
19. J. Ritman et al., Z. Phys. A **352**, 355 (1995).
20. G.Q. Li et al., Phys. Rev. Lett. **74**, 235 (1995); Phys. Lett. B **381**, 17 (1996).
21. P. Braun-Munzinger, J. Stachel, J.P. Wessels, N. Xu, Phys. Lett. B **344**, 43 (1995).
22. J. Cleymans, H. Oeschler, K. Redlich, Phys. Rev. C **59**, 1663 (1999).
23. S. Schnetzer et al., Phys. Rev. Lett. **49** 989 (1982); Phys. Rev. C **40**, 640 (1989).
24. A. Shor et al., Phys. Rev. Lett. **63**, 2192 (1989).
25. A. Schröter et al., Z. Phys. A **350**, 101 (1994).
26. P. Senger et al., Nucl. Instrum. Methods A **327**, 393 (1993).
27. D. Miśkowiec et al., Nucl. Instrum. Methods A **350**, 174 (1994).
28. J. Hüfner, J. Knoll, Nucl. Phys. A **290**, 460 (1977).
29. J. Balewski et al., Phys. Lett. B **388**, 859 (1996); Phys. Lett. B **420**, 211 (1998).
30. R. Averbeck et al., Z. Phys. A **359**, 215 (1977).
31. C.B. Dover, G.E. Walker, Phys. Rep. **89**, 1 (1982).
32. A. Sibirtsev, W. Cassing, C.M. Ko, Z. Phys. A **358**, 101 (1997).
33. E. Bratkovskaya, W. Cassing, U. Mosel, Nucl. Phys. A **622**, 593 (1997).
34. A. Sibirtsev, Phys. Lett. B **359**, 29 (1995).
35. F. Balestra et al., Phys. Lett. B **468**, 7 (1999).
36. C. Fuchs et al., Phys. Rev. C **56**, R606 (1997).
37. E. Bratkovskaya, W. Cassing, private communication
38. C. Fuchs, J. Aichelin, private communication